*Article*

# Solvothermal Synthesis of LaF₃:Ce Nanoparticles for Use in Medicine: Luminescence, Morphology and Surface Properties

**Anastasiia Dorokhina** [1,2,3,*]**, Ryoya Ishihara** [1]**, Hiroko Kominami** [1]**, Vadim Bakhmetyev** [3] **, Maxim Sychov** [3]**, Toru Aoki** [1,4] **and Hisashi Morii** [4]

[1] Research Institute of Electronics, Shizuoka University, Hamamatsu 432-8011, Japan
[2] Graduate School of Science and Technology, Shizuoka University, Hamamatsu 432-8011, Japan
[3] Saint-Petersburg State Institute of Technology, St. Petersburg 190013, Russia
[4] ANSeeN Inc., Hamamatsu 432-8003, Japan
[*] Correspondence: nastya.dorokhina@mail.ru

**Abstract:** A series of LaF₃:Ce³⁺ phosphors for application in photodynamic therapy are synthesized using a one-stage solvothermal synthesis. The synthesis conditions; type and quantity of stabilizer; concentration of activator providing the maximum intensity of UV- and X-ray-excited luminescence; lowest size; and highest colloidal stability of the phosphor nanoparticles are found. As a result of this study, the following parameters are determined using cerium content 5% mol. ethanol as the reaction medium for the solvothermal synthesis and polyvinylpyrrolidone as the stabilizer at an optimized amount.

**Keywords:** X-ray luminescence; solvothermal synthesis; LaF₃:Ce; zeta-potential; PEG; PVP; PEI

## 1. Introduction

Fluorides have many advantages as fluorescent raw materials due to their low phonon energy and high ionicity [1]. Compared with oxide luminescent materials, rare earth fluorides have optical clarity, low vibrational energy, minimal dopant ion excited state quenching and are also less prone to staining due to the formation of hole centers under the action of an ionizing emitter [2]. Fluoride nanocrystals doped with rare earth ions are of great interest due to their potential applications in lighting and displays [3–7], boost converters [8,9], biological fluorescent labels [10,11], transparent glass [12], scintillators [13], optical amplifiers [14], solar cell amplification [15] and photodynamic therapy [16,17]. Recently, some researchers have devoted themselves to the development of LaF₃ nanocrystals doped with rare earth ions due to their high photochemical stability, low toxicity and biocompatibility. In addition, their luminescent properties, including sharp absorption and emission lines and long lifetimes, are almost independent of particle size and can be tuned through doping with various lanthanide ions [18]. Ce³⁺ is a strong emitter with a nanosecond luminescence lifetime that is shorter than rare earth elements with 4f configurations due to the allowed 5d-4f optical transition, which is independent of crystal field state mixing due to its dipole nature. Although the ion–lattice interaction for the 5d configuration is higher than for the 4f configuration, nonradiative decay with multiphonon emission is impossible due to the large distance between the 5d band and the nearest 4f level [19–21]. LaF₃, which has a large band gap (according to various sources: from 6.04 eV [22] to 10.1 eV [23]), is an ideal host for Ce³⁺ scintillator fluorescence since the 4f and 5d levels of cerium are located in the gap receiving grid. In addition, since interactions between lanthanum and cerium ions have very similar chemical properties, the interaction between optically active Ce³⁺ ions can be reduced by replacing these ions with La³⁺ ions [24].

The agglomeration of LaF₃ nanocrystals doped with lanthanide ions is very common firstly because of the reduced open surface in nanocrystals, which reduces surface energy, and secondly because, as a rule, nanocrystals that do not have a special coating have a surface charge closer to neutral, which leads to the aggregation and flocculation of particles due to the action of van der Waals forces of attraction on them. This can lead to physical

instability [25,26]. To increase biocompatibility, as well as to prevent agglomeration, the particles are coated with various stabilizers. The most widely used and studied stabilizer is polyethylene glycol (PEG). The process of applying a PEG coating to biomaterials to impart a latent characteristic is commonly referred to as PEGylation. It is now well known that PEGylation has many attractive properties; for example, it has been shown to increase the half-life of a drug in the body, prolonging its potency and thus reducing dosing frequency. The ability of PEG to prolong carrier circulation time is mainly due to its physical properties, which, in turn, can reduce or prevent protein absorption. It has been approved by the FDA for use in a variety of dosage forms. PEGylation remains the reference process for the development of biologically relevant systems with in vivo characteristics. However, the disadvantages of this stabilizer have also become known: a long elimination time; lack of biodegradability; the formation of undesirable by-products; and mechanical degradation [27]. Alternatively, polyethyleneimine and polyvinylpyrrolidone have also been successfully used as stabilizers.

Oncological diseases in terms of prevalence and mortality occupy one of the leading places among socially significant pathologies. Many types of oncological tumors are resistant to certain types of anticancer therapy; thus, the development of new types of therapy is an extremely important task, especially for the development of personalized medicine approaches. Photodynamic therapy (in the optical range of radiation) has recently been increasingly used to treat a number of types of oncological tumors with shallow localization. However, due to the small depth of the penetration of optical radiation into B tissue, this method has significant limitations in terms of the area of the localization of pathogenic tissues in the body.

The X-ray photodynamic therapy (XPDT) method makes it possible to overcome the above limitations; however, in order to ensure the efficient adsorption and subsequent transformation of X-ray energy, materials for (XPDT) are usually designed on the basis of toxic heavy elements. The objective of this project is to develop effective nanocomposite materials for XPDT applications with improved biocompatibility parameters.

In the previous years of project implementation, syntheses of a wide range of X-ray phosphors have been carried out, including those based on matrices such as $Y_2O_3$ [28] and $Na_3PO_4$ [29], as well as the further creation of composites based on them. However, samples of nanocomposites based on fluorides and rare-earth elements such as lantanium and yttrium proved to be the most effective for the needs of XPDT. At the same time, the presence of such elements in the system makes it possible to use the developed nanocomposites for processes such as CT and MRI imaging.

This study is related to the improvement of the parameters of the process used for the synthesis of $LaF_3$ nanocrystals using the solvothermal method. The influence of the reaction medium and stabilizers on the structural, morphological and surface properties are studied using appropriate mathematical and analytical methods. Then, $Ce^{3+}$ ions of the optimal concentration are doped into the optimal host nanomaterial, and the optical characteristics for medical applications are studied.

## 2. Materials and Methods

A series of fluoride phosphors with the composition $LaF_3:Ce^{3+}$ 4 … 6% mol. was synthesized using the solvothermal method to determine the optimal concentration of $Ce^{3+}$. Ordinarily, the synthesis is carried out in organic solvents to provide electrostatic and electrosteric interaction between individual particles and thus prevent their aggregation [30]. A typical synthesis [31] was carried out in ethylene glycol. Water solution of cerium and lanthanum chlorides (8 mmol) was well mixed and added to ethylene glycol. After adding stabilizer polyethylene glycol Mw = 20,000 (PEG-20000), the mixture was vigorously stirred on a magnetic stirrer at room temperature. Ammonium fluoride $NH_4F$ (12 mL of 110 mol. solution) was dissolved in ethylene glycol, added to the above solution and again stirred vigorously at room temperature for 30 min. Finally, the mixture was transferred to a Teflon liner and placed in a sealed stainless-steel autoclave, where it was

subjected to a solvothermal treatment at 200 °C for 4 h and was then cooled naturally to room temperature. The precipitate was washed in ethanol and deionized water several times, and the final products were dried at 40 °C for 6 h in a normal atmosphere.

To determine the most suitable synthesis media, a series of samples was synthesized by the earlier described method, but in the case of synthesis in ethanol, medium ammonium fluoride was dissolved in DI water. For this series, the same stabilizer (PEG-20000), synthesis parameters (200 °C, 4 h) and the same concentration of $Ce^{3+}$ (5% mol.) for all the samples were applied.

To determine the optimal stabilizer that would prevent particle coalescence and ensure biocompatibility, $LaF_3$:$Ce^{3+}$ nanocrystals were synthesized with various organic surfactants, including polyethylene glycol (PEG-200, PEG-2000, PEG-20000), polyethyleneimine (PEI Mw 60,000–80,000) and polyvinylpyrrolidone (PVP Mw 1,300,000), and the luminescent and surface properties of nanoparticles were investigated. The synthesis was carried out in ethanol medium at 200 °C for 4 h; all samples of this series had a cerium concentration of 5% mol.

As a result of the previous series of syntheses, PVP was chosen as the optimal stabilizer for $LaF_3$:Ce nanocrystals. The next step was to study the optimal amount of PVP. A total of 4 samples were synthesized with the amount of PVP ranging from 0 to 1.5 g. Synthesis was carried out using the same parameters as in previous series (200 °C, 4 h, ethanol medium).

The structural characteristics of the final products were investigated by powder X-ray diffraction (XRD) using Cu-Ka radiation (l = 0.15405 nm) on a Rigaku-RINT2200 diffractometer. The morphologies and sizes of the obtained samples were observed using field emission scanning electron microscope (FE-SEM, JSM-7001F, JEOL). Size distribution histograms were obtained using ImageJ software. Four images were taken for each sample to calculate average size and size distribution. The emission spectra of ultraviolet and visible photoluminescence were recorded using a laboratory setup: a spectrofluorometer with two monochromators (model of an ultramonochromatic light source) equipped with a xenon lamp as an exciter. The emission and excitation spectra were obtained with excitation photons from Beamline 3B of the Ultraviolet Synchrotron Orbital Radiation Facility III (UVSOR-III) at a temperature of 7 K using liquid helium. The X-ray luminescence spectra were measured on a laboratory setup with a copper anode at a voltage of 80 kV and a current of 62 mA. FTIR spectrum is recorded between 4000 and 400 $cm^{-1}$. Dried samples were measured with FT/IR-6300, JASCO. Surface charge and size distribution of the samples were measured with Zetasizer Ultra and analyzed with ZS Xplorer software by Malvern Pnalytical. All measurements were carried out at room temperature. The Vienna ab initio simulation package (VASP) within the DFT framework for full structure optimizations and total energy calculations was employed [32,33].

## 3. Results and Discussion

To determine the optimal concentration of cerium, a series of syntheses of the samples with a concentration of 4 … 6 mol% was carried out. Figure 1 shows the XRD patterns of the obtained samples. The structure of the obtained $LaF_3$:$Ce^{3+}$ nanoparticles was in good agreement with the hexagonal structure of bulk $LaF_3$ (card 72-1435). The diffraction peaks for all the samples were broadened, which indicates the nanocrystalline nature of the samples. The average crystallite sizes were estimated from the Scherrer equation [34],

$$Dhkl = k\lambda / \beta \cos\Theta \qquad (1)$$

where $k = 1$, $\lambda = 0.154184$ nm represents the wavelength of Cu *K* radiation, $\Theta$ is the angle of the X-ray diffraction peak and $\beta$ represents the corrected half width of the diffraction peak. Taking the 9 main peaks (002, 110, 111, 112, 300, 113, 220, 221, 223), the average crystallite sizes of $LaF_3$:4%$Ce^{3+}$, $LaF_3$:5%$Ce^{3+}$ and $LaF_3$:6%$Ce^{3+}$ were about 25.1, 31.9 and 33.1 nm, respectively. Figure 1b shows the peak (111) at $2\Theta = 27.6°$; it can be seen that with the increase in the concentration of cerium, the peak shifts towards lower degrees, which indicates an increase in the amount during the cerium fluoride phase.
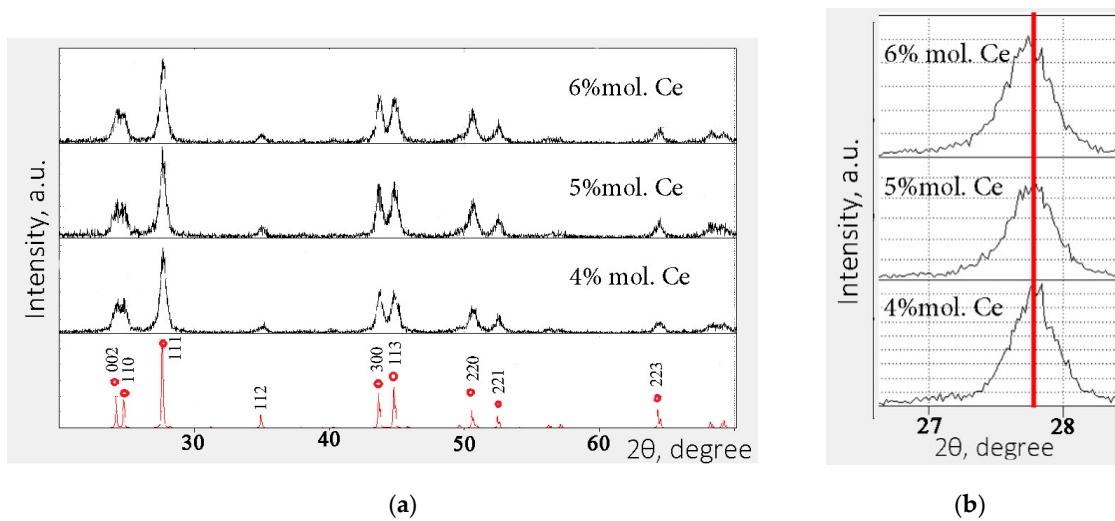
**Figure 1.** XRD patterns of LaF$_3$:Ce (**a**) with different Ce$^{3+}$ concentration; (**b**) XRD peak (111) at 27.6°.

Figure 2 shows the photo and X-ray luminescence spectra of LaF$_3$:Ce phosphors with different activator concentrations. Photoluminescence was measured at room temperature with an excitation wave of 255 nm (Figure 2a).

Broadband radiation in the region from 270 to 400 nm and peaking at 300 nm can be attributed to the 5d–4f transition of Ce$^{3+}$. With the increase in the doping concentration of Ce$^{3+}$, the radiation intensity gradually increases, reaching a maximum at a concentration of 5% mol., and then decreases. The decrease in radiation intensity was related to the concentration effect of quenching at a higher doping concentration of Ce$^{3+}$. A similar behavior was also observed upon X-ray excitation (Figure 2b).

It is known that the luminescence spectra of trivalent lanthanide ions are mainly due to two types of electronic transitions: the 4f–4f transition and the 5d–4f transition. The excited electronic configuration of Ce$^{3+}$ has the form 5d$^1$ and is not shielded from the surroundings. The 5d electron interacts strongly with neighboring anion ligands in compounds, which leads to broadband emission. The 4f orbital is shielded from the environment by the filled 5s$^2$ and 5p$^6$ orbitals. Thus, the effect of the main lattice on optical transitions within the 4f$^n$ configuration is small [35].
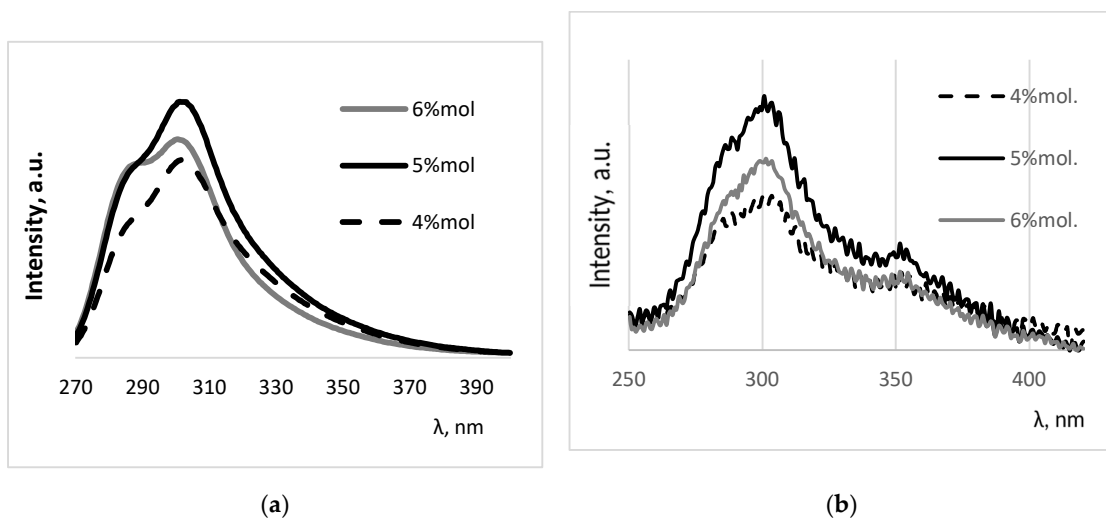


**Figure 2.** Photoluminescent (**a**) and X-ray luminescent (**b**) spectra of LaF$_3$:Ce with different Ce$^{3+}$ concentrations.

It is important to use the correct technique to synthesize nanoparticles for a medical application because each nanoparticle must have the appropriate morphology for the desired application. It is known that toxicity increases from spherical to acicular particles [36]. It is therefore very important to synthesize nanosized particles and also, if possible, to produce their ideal shape. We thought that solvothermal methods would control the morphology to an appropriate degree. When conducting a solvothermal reaction, many factors must be taken into account, such as the concentrations of the reactants, the solubility of the reactants, the reaction temperature, the reaction time, the choice of solvent and the pressure, all of which can be varied. In our previous papers, we have already discussed the optimal parameters for the synthesis of yttrium fluoride [37]. In this article, we paid special attention to the solvent used as the reaction medium. In this case, we used ethanol and ethylene glycol (EG).

The solvothermal reaction was carried out at 200 °C for 4 h using PEG-20000 as a stabilizer and with a cerium concentration of 5% mol. As a result of synthesis using these reaction media, pure hexagonal lanthanum fluoride was obtained (Figure 3). Thus, it can be concluded that the synthesis medium does not affect the formation of the phase. This statement was also confirmed for us in [37].
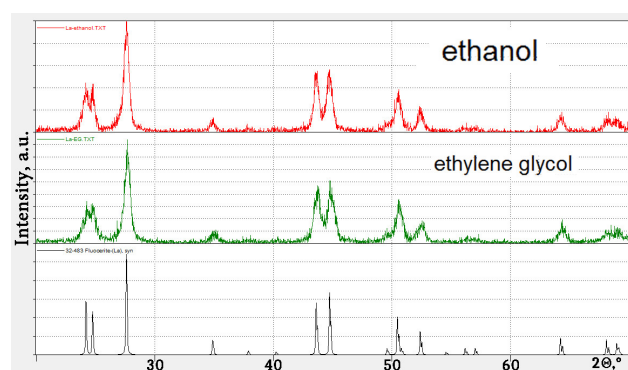


**Figure 3.** XRD patterns of LaF$_3$:Ce synthesized in various media.

Figures 4 and 5 show SEM images and size distribution histograms calculated from the acquired images, respectively.

The shape of nanoparticles can affect their biocompatibility and toxicity. This was illustrated by a change in the shape of the material from equiaxed to acicular, after which the toxic reaction intensified [38]. This may have been due to the interaction forces of longitudinally oriented nanomaterials, which increase in proportion to their length. Consequently, the van der Waals forces for rod nanomaterials are greater than for spherical ones. The shape of nanomaterials can also influence the rate of cell internalization. Spherical particles penetrate the cell membrane more easily than particles with a large length-to-radius ratio (elongated) lying parallel to the cell membrane. For example, spherical gold nanoparticles absorb more than their rod counterparts. Therefore, the nanomaterials can be shaped appropriately to more easily enter cells for therapeutic purposes such as cancer therapy.

SEM images (Figure 4) show that the obtained particles were oval in shape and did not exceed nanosize. These samples are also histograms in Figure 5, which were read from the acquired images using the software. It should be noted that the synthesis medium had practically no effect on the particle morphology; however, a narrower particle size distribution was obtained as a result of synthesis in an ethanol medium. Furthermore, in this medium, as the calculations show, it is possible to obtain an average particle size of about 30 nm, while in an ethylene glycol (EG) medium, the average size is about 45 nm. Thus, ethanol was chosen as the reaction medium for the solvothermal synthesis of lanthanum fluoride.
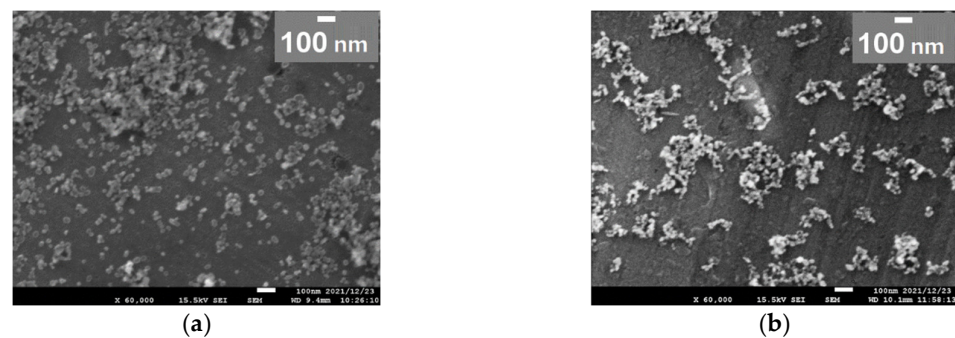
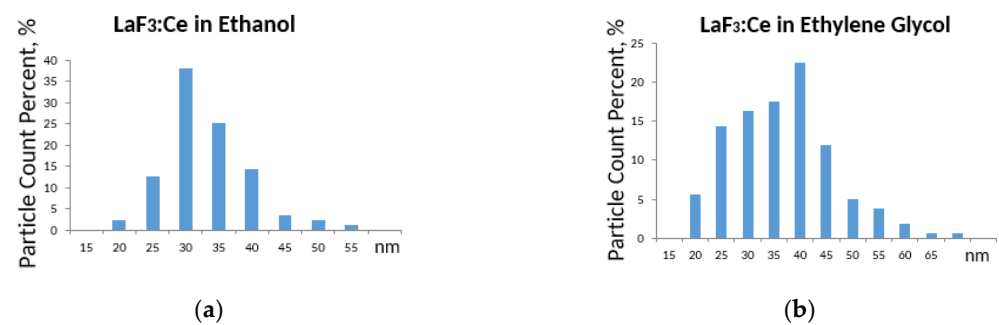**Figure 4.** SEM images of LaF$_3$:Ce 5% mol. synthesized in ethanol (**a**) and EG (**b**).



**Figure 5.** Size distribution of LaF$_3$:Ce 5% mol. synthesized in ethanol (**a**) and EG (**b**).

Nanoparticles must be stabilized with suitable compounds since a decrease in particle size increases the number of surface atoms and the surface energy of the formed particles [39]. Nanoparticles are stabilized before their actual use in any technological applications by modifying their surface with appropriate stabilizers. This surface modification with stabilizers (also called blocking ligands) is critical to achieving sufficient repulsive forces between particles that prevent particle aggregation and help obtain the stable suspension of particles. A special polymer coating allows for higher biocompatibility, prevents agglomeration and also makes it possible to obtain a stable colloidal nanosuspension. We synthesized a series of samples with various stabilizers: polyethylene glycol (PEG) with Mw 200 and 2000, polyvinylpyrrolidone (PVP) and polyethyleneimine (PEI). PEG and PVP belong to a steric model of stabilization [40,41]. It is worth noting that the sheath is usually not a continuous impermeable layer, but rather a discontinuous layer. Thus, there is an interaction between the nucleus and the environment. Heterogeneity arises from steric and electrosteric forces between macromolecules attached to the surface. At present, the control of the morphology and size of fluoride nanoparticles during their preparation is an important factor that needs to be addressed for their use in medicine.

The functional groups of the samples were measured using FT-IR as shown in Figure 6. A broad absorption band of around 3500–3400 cm$^{-1}$ is related to stretching vibrations (-OH). In the spectrum of PEG-200 and PEG-2000, characteristic bands at 2874.2 cm$^{-1}$ and at 1103.9 cm$^{-1}$ of certain functional groups were found belonging to the –CH group [42] and the –C–O–C group [43], respectively. The appearance of these two characteristic bands and some other bands near 1103.9 cm$^{-1}$ in the PEG–LaF$_3$:Ce spectrum indicated the successful conjugation of PEG to the LaF$_3$:Ce surface. The spectrum of PEI shows a few weak peaks in the 1170–1050 cm$^{-1}$ range that correspond to C-O, C-C and C-O-C stretching vibrations (associated with carbo-hydrate ring), and presence of C-N stretching is characteristic of PEI. The large band at 1632–1622 cm$^{-1}$ may have been due to C=O asymmetric stretching in (COO−), (-N-H) bending vibration (for primary and secondary amines) and/or open-chain amino groups (-C=N-). In addition, in the region 2980–2850 cm$^{-1}$ stretching vibrations of -CH bonds appeared, which confirmed the expected presence of linear aliphatic chains. The spectrum of PVP had characteristic peaks C=O (1660 cm$^{-1}$) and C-N (1290 cm$^{-1}$), which confirmed the functionalization of PVP lanthanum fluoride nanoparticles through intermolecular hydrogen bonding.
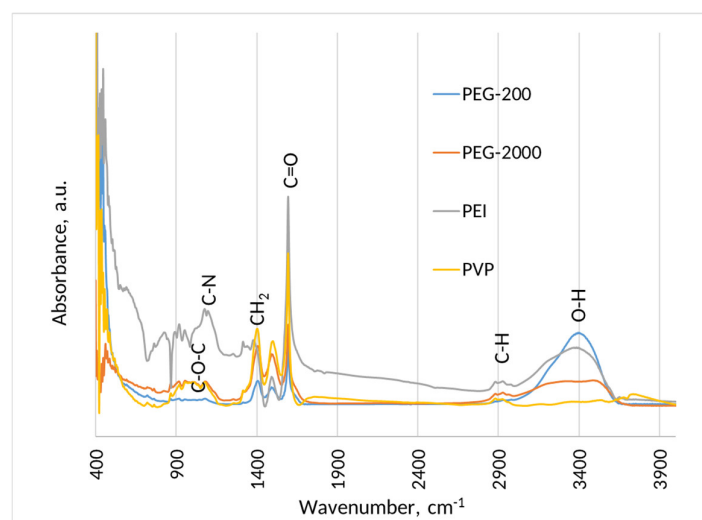
**Figure 6.** FT-IR spectra of LaF$_3$:Ce with different stabilizers.

Particles with a zeta-potential of $\pm30$ mV have an optimal surface charge, which is acceptable for biocompatibility [44]. Typically, zeta-potential values are in the range of +100 to −100 mV. A high value for the zeta-potential of nanoparticles indicates the good physical stability of nanosuspensions due to the electrostatic repulsion of individual particles. A zeta-potential value other than one between −30 mV and +30 mV is generally considered to have sufficient repulsive force to achieve better physical colloidal stability. A low zeta-potential can lead to physical instability due to particle aggregation and flocculation due to van der Waals attractive forces acting on them [45]. However, surface charge affects the behaviors of particles with biological constituents, such as cell-to-cell interactions, permeation, protein adsorption and stability in biological fluid. Neutral particles show a slower opsonization rate than charged particles, and nanoparticles with small negative charges tend to accumulate more efficiently in tumor tissues. Positively charged particles can be more easily taken up by cells than other nanoparticles due to the attractive interaction between positively charged nanoparticles and negative cell membranes. On the other hand, cationic nanoparticles are much more effective in activating the immune response than neutral or anionic nanoparticles.

As can be seen from Figure 7, PEG-coated particles have an extremely positive charge, which can be as high as 70 mV. In the case of PEI, the particles have both positive and negative charges, which directly leads to a high probability of agglomeration. PVP has positively charged particles, most of which have a charge of about 40 mV, which is close to the optimum particle charge to achieve colloidal stability. Thus, PVP was chosen as a suitable stabilizer.

After determining the optimal surfactant, an experiment was conducted to determine the optimal amount of PVP. Four samples were synthesized with different PVP quantities: 0 g, 0.375 g, 0.75 g and 1.5 g. Figure 8a shows the diffraction patterns of the obtained samples. As noted earlier, the presence of surfactants does not affect the phase composition. Therefore, it is possible to observe hexagonal lanthanum and cerium fluoride without impurity phases.

Figure 8b shows the excitation and luminescence spectra of the obtained samples measured at the temperature of 7 K using liquid helium. Peaks located in the region of 90–150 nm were related to the excitation of the phosphor host lanthanum fluoride. The bandgap for LaF$_3$ was calculated using the VASP method [46], and it was equal to 8.3 eV (Figure 9), which correlated with the obtained excitation spectra peak at 125 nm (9.9 eV). For the total energy calculations, the Vienna ab initio (VASP) DFT simulation package was used. A basis set of plane waves and extended projector wave (PAW) potentials were used to determine the electronic wave functions [47]. A $2 \times 2 \times 2$ supercell (192 atoms–8 unit cells of hexagonal LaF$_3$) was first optimized using the Perdew–Burke–Ernzerhof (PBE) exchange and correlation functional. The larger supercell was not tested; since the LaF$_3$

matrix is not complicated (only 2 types of atoms), we assumed that the error of calculation would be very small as the difference in formation energy was found to be less than 3%, which indicates that the effect of supercell size is negligible [46].
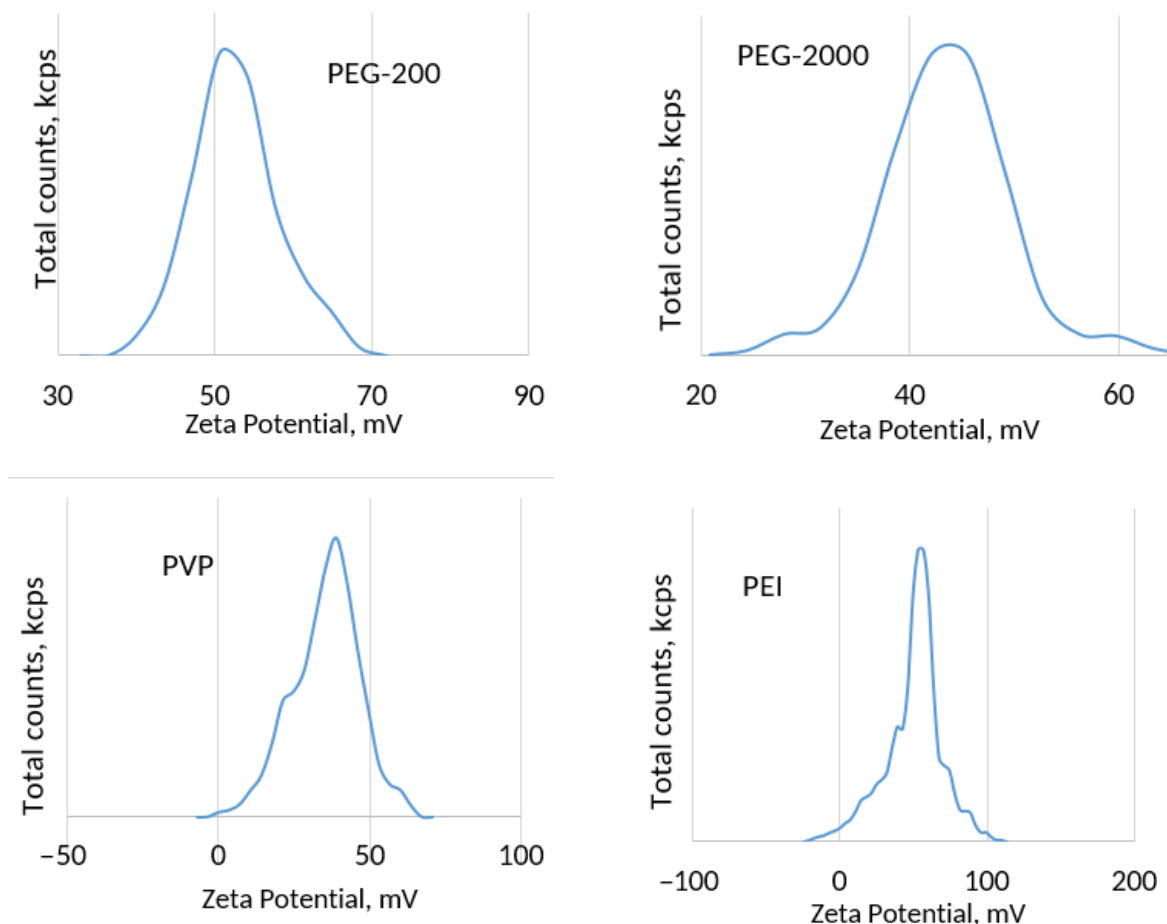


**Figure 7.** Zeta-potential of LaF$_3$:Ce 5% mol. with different stabilizers.

As can be seen from the excitation spectra, the main peaks, in contrast to the emission spectra, were not elementary. Conditioned to 4f–5d transition peaks in the excitation spectra at 191.5, 206, 214, 229 and 246 nm correlated with the maxima of 5d$^1$–5d$^5$ of the cerium luminescence in LaF$_3$:Ce [48]. The emission spectra of the obtained samples demonstrated the same pattern as the samples obtained earlier. The sample with a PVP content of 0.75 g had the highest intensity.

The nature of the peak at 114 nm (Figure 8b) could be associated with the formation of exciton states corresponding to the 2pF$^-$→5d$^2$ transitions. There was no exciton luminescence associated with the appearance of an anionic exciton, which was possibly due to the deactivation of the 2pF$^0$ hole states by electronic transitions from 4fCe$^{3+}$ [49].

The lower part of Figure 8b shows the luminescence spectrum of LaF$_3$:Ce taken at 70 nm excitation wavelength. As can be seen from the spectra, the main peaks at 292 nm and 310 nm were located at the same wavelength as at 255 nm excitation. However, the intensity ratios of the peaks were different, which can be explained by the fact that since the excitation wavelength was shorter, the luminescent peak with a shorter wavelength became more intense in comparison to, in this case, the peak at 310 nm.
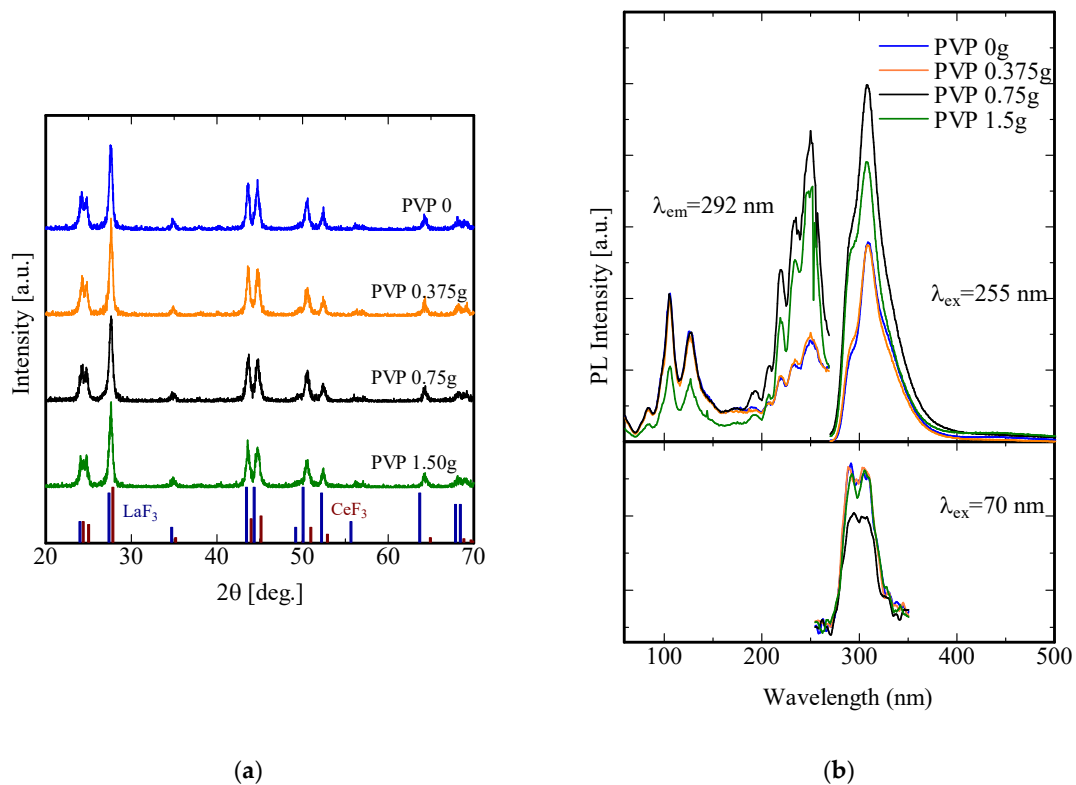
**(a)**                                **(b)**

**Figure 8.** XRD patterns (**a**) and photoluminescent spectra (**b**) of LaF$_3$:Ce with different quantities of PVP.
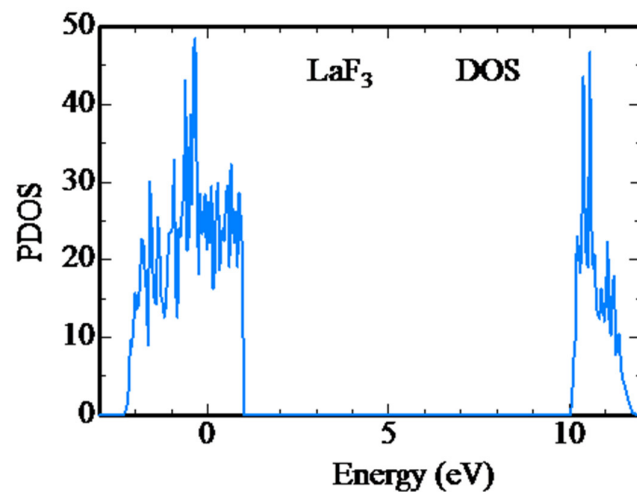


**Figure 9.** Total density of states (DOS) LaF$_3$ with calculated E$_g$ = 8.3 eV.

## 4. Conclusions

As a result of the performed studies, a one-stage solvothermal procedure was developed and optimized for obtaining Ce$^{3+}$-doped LaF$_3$ nanoparticles, which appears promising as an efficient phosphor for medical usage, in particular for the photodynamic therapy of cancer. Ce$^{3+}$ concentration 5 mol. % afforded the highest luminescence intensity upon UV and X-ray excitation. A theoretical calculation of the valence band of LaF$_3$ was made, which coincided with the practical result obtained. The wasted volume of the LaF$_3$ valence band was 8.3 eV, which corresponded to the 125 nm band of the excitation spectrum. The lowest phosphor particle size of about 30 nm convenient for PDT application was achieved in using ethanol as the reaction medium for the synthesis. The application of polyvinylpyrrolidone as a stabilizer at an optimized amount provided the optimal zeta-potential and charge of the phosphor

nanoparticles, affording the stabilization of their colloidal solutions. The developed approach is promising for implementation in the commercial production of non-toxic water-soluble luminescent $LaF_3$:Ce nanoparticles useful in photodynamic therapy and other applications, including various biological experiments.

**Author Contributions:** Conceptualization, A.D., H.K. and M.S.; methodology, H.K., V.B. and A.D.; investigation, A.D., R.I. and H.K.; resources, H.K., T.A. and H.M.; writing—original draft preparation, A.D.; writing—review and editing, H.K. All authors have read and agreed to the published version of the manuscript.

**Conflicts of Interest:** The authors declare no conflict of interest.

## References

1. Yan, R.X.; Li, Y.D. Down/Up Conversion in $Ln^{3+}$-Doped $YF_3$ Nanocrystals. *Adv. Funct. Mater.* **2005**, *15*, 763. [CrossRef]
2. Tan, M.C.; Al-Baroudi, L.; Riman, R.E. Surfactant effects on efficiency enhancement of infrared-to-visible upconversion emissions of $NaYF_4$:Yb-Er. *Appl. Mater. Interfaces* **2011**, *3*, 3910–3915. [CrossRef] [PubMed]
3. Wang, Z.L.; Chan, H.L.W.; Li, H.L.; Hao, J.H. Highly efficient low-voltage cathodoluminescence of $LaF_3$:$Ln^{3+}$ (Ln=$Eu^{3+}$, $Ce^{3+}$, $Tb^{3+}$) spherical particles. *Appl. Phys. Lett.* **2008**, *93*, 141106. [CrossRef]
4. Jia, P.; Lin, J.; Yu, M. Sol–gel deposition and luminescence properties of $LiYF_4$:$Tb^{3+}$ thin films. *J. Lumin.* **2007**, *122–123*, 134–136. [CrossRef]
5. Tuyet, D.T.; Quan, V.T.; Bondzior, B.; Dereń, P.J.; Velpula, R.T.; Nguyen, H.P.; Tuyen, L.A.; Hung, N.Q.; Nguyen, H.D. Deep red fluoride dots-in-nanoparticles for high color quality micro white light-emitting diodes. *Opt. Express* **2020**, *28*, 26189–26199. [CrossRef]
6. Kemnitz, E.; Mahn, S.; Krahl, T. Nano metal fluorides: Small particles with great properties. *ChemTexts* **2020**, *6*, 19. [CrossRef]
7. Quan, Z.; Yang, D.; Yang, P.; Zhang, X.; Lian, H.; Liu, X.; Lin, J. Uniform Colloidal Alkaline Earth Metal Fluoride Nanocrystals: Nonhydrolytic Synthesis and Luminescence Properties. *Inorg. Chem.* **2008**, *47*, 9509–9517. [CrossRef]
8. Heer, S.; Kömpe, K.; Güdel, H.U.; Haase, M. Highly Efficient Multicolour Upconversion Emission in Transparent Colloids of Lanthanide-Doped $NaYF_4$ Nanocrystals. *Adv. Mater.* **2004**, *16*, 2102. [CrossRef]
9. Schietinger, S.; Menezes, L.S.; Lauritzen, B.; Benson, O. Observation of Size Dependence in Multicolor Upconversion in Single $Yb^{3+}$, $Er^{3+}$ Codoped $NaYF_4$ Nanocrystals. *Nano Lett.* **2009**, *9*, 2477–2481. [CrossRef]
10. Yi, G.S.; Lu, H.C.; Zhao, S.Y.; Ge, Y.; Yang, W.J.; Chen, D.P.; Guo, L.H. Synthesis, Characterization, and Biological Application of Size-Controlled Nanocrystalline $NaYF_4$:Yb,Er Infrared-to-Visible Up-Conversion Phosphors. *Nano Lett.* **2004**, *4*, 2191–2196. [CrossRef]
11. Nam, S.H.; Bae, Y.M.; Park, Y.I.; Kim, J.H.; Kim, H.M.; Choi, J.S.; Lee, K.T.; Hyeon, T.; Suh, Y.D. Long-term real-time tracking of lanthanide ion doped upconverting nanoparticles in living cells. *Angew. Chem. Int. Ed. Engl.* **2011**, *50*, 6093–6097. [CrossRef]
12. Zhou, S.F.; Jiang, N.; Miura, K.; Tanabe, S.; Shimizu, M.; Sakakura, M.; Shimotsuma, Y.; Nishi, M.; Qiu, J.R.; Hirao, K. Simultaneous Tailoring of Phase Evolution and Dopant Distribution in the Glassy Phase for Controllable Luminescence. *J. Am. Chem. Soc.* **2010**, *132*, 17945–17952. [CrossRef]
13. Wang, Z.L.; Quan, Z.W.; Jia, P.Y.; Lin, C.K.; Luo, Y.; Chen, Y.; Fang, J.; Zhou, W.; O'Connor, C.J.; Cerium, J.L. III Fluoride Thin Films by XPS. *Chem. Mater.* **2006**, *18*, 2030. [CrossRef]
14. Sivakumar, S.; van Veggel, F.C.J.M.; Raudsepp, M. Bright White Light through Up-Conversion of a Single NIR Source from Sol−Gel-Derived Thin Film Made with $Ln^{3+}$-Doped $LaF_3$ Nanoparticles. *J. Am. Chem. Soc.* **2005**, *127*, 12464–12465. [CrossRef]
15. Liu, S.M.; Chen, W.; Wang, Z.G. Luminescence Nanocrystals for Solar Cell Enhancement. *J. Nanosci. Nanotechnol.* **2010**, *10*, 1418–1429. [CrossRef]
16. Liu, Y.F.; Chen, W.; Wang, S.P.; Joly, A.G. Investigation of water-soluble x-ray luminescence nanoparticles for photodynamic activation. *Appl. Phys. Lett.* **2008**, *92*, 043901. [CrossRef]
17. Chen, W. Nanoparticle Self-Lighting Photodynamic Therapy for Cancer Treatment. *J. Biomed. Nanotechnol.* **2008**, *4*, 369–376. [CrossRef]
18. Wang, F.; Han, Y.; Lim, C.S.; Lu, Y.; Wang, J.; Xu, J.; Chen, H.; Zhang, C.; Hong, M.; Liu, X. Simultaneous phase and size control of upconversion nanocrystals through lanthanide doping. *Nature* **2010**, *463*, 1061–1065. [CrossRef]

19. Moses, W.; Derenzo, S.; Weber, M.; Ray-Chaudhuri, A.; Cerrina, F. Scintillation mechanisms in cerium fluoride. *J. Lumin.* **1994**, *59*, 89–100. [CrossRef]

20. Yao, M.; Joly, A.G.; Chen, W. Formation and Luminescence Phenomena of $LaF_3:Ce^{3+}$ Nanoparticles and Lanthanide−Organic Compounds in Dimethyl Sulfoxide. *J. Phys. Chem. C* **2010**, *114*, 826–831. [CrossRef]

21. Birowosuto, M.D.; Dorenbos, P.; van Eijk, C.W.E.; Krmer, K.W.; Gudel, H.U. Scintillation properties and anomalous $Ce^{3+}$ emission of $Cs_2NaREBr_6:Ce^{3+}$ (RE = La,Y,Lu). *J. Phys. Condens. Matter* **2006**, *18*, 6133. [CrossRef] [PubMed]

22. Petousis, I.; Mrdjenovich, D.; Ballouz, E.; Liu, M.; Winston, D.; Chen, W.; Graf, T.; Schladt, T.D.; Persson, K.A.; Prinz, F.B. High-throughput screening of inorganic compounds for the discovery of novel dielectric and optical materials. *Sci. Data* **2017**, *4*, 160134. [CrossRef] [PubMed]

23. Tabatabaee, F.; Sabbagh Alvani, A.A.; Sameie, H.; Moosakhani, S.; Salimi, R.; Taherian, M. $Ce^{3+}$-doped $LaF_3$ nanoparticles: Wet-chemical synthesis and photo-physical characteristics "optical properties of $LaF_3:Ce$ nanomaterials". *Met. Mater. Int.* **2014**, *20*, 169–176. [CrossRef]

24. Canning, A.; Chaudhry, A.; Boutchko, R.; Gronbech-Jensen, N. First-principles study of luminescence in Ce-doped inorganic scintillators. *Phys. Rev.* **2011**, *83*, 125115. [CrossRef]

25. Freitas, C.; Müller, R.H. Müller Spray-drying of solid lipid nanoparticles (SLNTM). *Eur. J. Pharm. Biopharm.* **1998**, *46*, 145–151. [CrossRef]

26. Shah, S.; McRae, A.F.; Marioni, R.E.; Harris, S.E.; Gibson, J.; Henders, A.K.; Redmond, P.; Cox, S.R.; Pattie, A.; Corley, J.; et al. Genetic and environmental exposures constrain epigenetic drift over the human life course. *Genome Res.* **2014**, *24*, 1725–1733. [CrossRef]

27. Zhang, F.; Liu, M.R.; Wan, H.T. Discussion about Several Potential Drawbacks of PEGylated Therapeutic Proteins. *Biol. Pharm. Bull.* **2014**, *37*, 335–339. [CrossRef]

28. Vlasenko, A.B.; Dorokhina, A.M.; Bakhmetyev, V.V.; Khristyuk, N.A.; Mjakin, S.V.; Kuzina, E.N.; Sychov, M.M.; Kominami, H.; Toru, A.; Morii, H. Hydrothermal synthesis and characterization of nano-sized phosphors based on rare-earth activated yttrium compounds for photodynamic therapy. *J. Sol-Gel Sci. Technol.* **2023**, 1–18. [CrossRef]

29. Viktorovich, M.V.; Vladimirovich, B.V.; Aleksandrovich, L.L. Synthesis and study of the properties of $nabapo_4:eu^{2+}$ phosphores of increased dispersion. *Izv. SPbGTI (TU)* **2017**, *65*.

30. Hotze, E.; Phenrat, T.; Lowry, G. Nanoparticle aggregation: Challenges to understanding transport and reactivity in the environment. *J. Environ. Qual.* **2010**, *39*, 1909–1924. [CrossRef]

31. Sudheendra, L.; Das, G.K.; Li, C.; Stark, D.; Cena, J.; Cherry, S.; Kennedy, I.M. $NaGdF_4:Eu^{3+}$ Nanoparticles for Enhanced X-ray Excited Optical Imaging. *Chem. Mater.* **2014**, *26*, 1881–1888. [CrossRef]

32. Rezende, M.V.d.S.; Araujo, R.M.; Valerio, M.E.G.; Jackson, R.A. Intrinsic Defects in Strontium Aluminates Studied via Computer Simulation Technique. *J. Phys. Conf. Ser.* **2010**, *249*, 012042. [CrossRef]

33. Kresse, G.; Joubert, D. From Ultrasoft Pseudopotentials to the Projector Augmented-Wave Method. *Phys. Rev. B* **1999**, *59*, 1758. [CrossRef]

34. Vinila, V.S.; Isac, J. *Design, Fabrication, and Characterization of Multifunctional Nanomaterials*; Elsevier: Amsterdam, The Netherlands, 2022.

35. Guo, H.; Zhang, T.; Qiao, Y.; Zhao, L.; Li, Z. Ionic Liquid-Based Approach to Monodisperse Luminescent $LaF_3:Ce,Tb$ Nan-odiskettes: Synthesis, Structural and Photoluminescent Properties. *J. Nanosci. Nanotechnol.* **2010**, *10*, 1913–1919. [CrossRef]

36. Nakashima, K.; Ueno, S.; Wada, S. Solvothermal synthesis of $KNbO_3$ nanocubes using various organic solvents. *J. Ceram. Soc. Jpn.* **2014**, *122*, 547–551. [CrossRef]

37. Dorokhina, A.M.; Bakhmetyev, V.V.; Kominami, H.; Toru, A.; Hisashi, M. Study of the properties of $Ce^{3+}$-doped fluoride nanophosphors: Phase composition, morphology, luminescence. *J. Phys. Conf. Ser.* **2021**, *2056*, 012048. [CrossRef]

38. Tarantola, M.; Pietuch, A.; Schneider, D.; Rother, J.; Sunnick, E.; Rosman, C.; Pierrat, S.; Sönnichsen, C.; Wegener, J.; Janshoff, A. Toxicity of gold-nanoparticles: Synergistic effects of shape and surface functionalization on micromotility of epithelial cells. *Nanotoxicology* **2011**, *5*, 254–268. [CrossRef]

39. Chaudhuri, R.G.; Paria, S. Core/Shell Nanoparticles: Classes, Properties, Synthesis Mechanisms, Characterization, and Applications. *Chem. Rev.* **2012**, *112*, 2373–2433. [CrossRef]

40. Varga, Z.; Wacha, A.; Vainio, U.; Gummel, J.; Bóta, A. Characterization of the PEG layer of sterically stabilized liposomes: A SAXS study. *Chem. Phys. Lipids* **2012**, *165*, 387–392. [CrossRef]

41. Römer, I.; White, T.; Baalousha, M.; Chipman, K.; Viant, M.; Lead, J. Aggregation and dispersion of silver nanoparticles in exposure media for aquatic toxicity tests. *J. Chromatogr. A* **2011**, *1218*, 4226–4233. [CrossRef]

42. Tolaymat, T.; El Badawy, A.; Genaidy, A.; Scheckel, K.; Luxton, T.; Suidan, M. An evidence-based environmental perspective of manufactured silver nanoparticle in syntheses and applications: A systematic review and critical appraisal of peer-reviewed scientific papers. *Sci. Total Environ.* **2010**, *408*, 999–1006. [CrossRef] [PubMed]

43. Petersen, H.; Fechner, P.M.; Martin, A.L.; Kunath, K.; Stolnik, S.; Roberts, C.J.; Fischer, D.; Davies, M.C.; Kissel, T. Polyethylenimine-graftpoly(ethylene glycol) copolymers: Influence of copolymer block structure on DNA complexation and biological activities as gene delivery system. *Bioconjug. Chem.* **2002**, *13*, 845–854. [CrossRef] [PubMed]

44. Samimi, S.; Maghsoudnia, N.; Eftekhari, R.B.; Dorkoosh, F. Chapter 3—Lipid-Based Nanoparticles for Drug Delivery Systems. In *Micro and Nano Technologies, Characterization and Biology of Nanomaterials for Drug Delivery*; Mohapatra, S.S., Ranjan, S., Dasgupta, N., Mishra, R.K., Thomas, S., Eds.; Elsevier: Amsterdam, The Netherlands, 2019; pp. 47–76.

45. Joseph, E.; Singhvi, G. Chapter 4—Multifunctional nanocrystals for cancer therapy: A potential nanocarrier. In *Nanomaterials for Drug Delivery and Therapy*; Grumezescu, A.M., Ed.; William Andrew Publishing: Norwich, NY, USA, 2019; pp. 91–116.

46. Finley, E.; Mansouri Tehrani, A.; Brgoch, J. Intrinsic Defects Drive Persistent Luminescence in Monoclinic $SrAl_2O_4$:$Eu^{2+}$. *J. Phys. Chem. C* **2018**, *122*, 16309–16314. [CrossRef]

47. Kresse, G.; Furthmüller, J. Efficient Iterative Schemes for ab initio Total-Energy Calculations Using a Plane-Wave Basis Set. *Phys. Rev. B Condens. Matter Mater. Phys.* **1996**, *54*, 11169–11186. [CrossRef]

48. Kochan, O.; Chornodolskyy, Y.; Selech, J.; Karnaushenko, V.; Przystupa, K.; Kotlov, A.; Demkiv, T.; Vistovskyy, V.; Stryhanyuk, H.; Rodnyi, P.; et al. Energy Structure and Luminescence of $CeF_3$ Crystals. *Materials* **2021**, *14*, 4243. [CrossRef]

49. Radzhabov, E.; Nepomnyashikh, A.I. F and Vk Centres in $LaF_3$, $CeF_3$ Crystals. 2015. Available online: http://arxiv.org/abs/1510.07781 (accessed on 30 June 2021).